

Multiple flaring activity in the supergiant fast X-ray transient IGR J08408–4503 observed with *Swift*

P. Romano,^{1*} L. Sidoli,² G. Cusumano,¹ P. A. Evans,³ L. Ducci,^{2,4} H. A. Krimm,^{5,6} S. Vercellone,² K. L. Page,³ A. P. Beardmore,³ D. N. Burrows,⁷ J. A. Kennea,⁷ N. Gehrels,⁶ V. La Parola¹ and V. Mangano¹

¹INAF, Istituto di Astrofisica Spaziale e Fisica Cosmica, Via U. La Malfa 153, I-90146 Palermo, Italy

²INAF, Istituto di Astrofisica Spaziale e Fisica Cosmica, Via E. Bassini 15, I-20133 Milano, Italy

³Department of Physics and Astronomy, University of Leicester, LE1 7RH

⁴Dipartimento di Fisica e Matematica, Università dell'Insubria, Via Valleggio 11, I-22100 Como, Italy

⁵Universities Space Research Association, Columbia, MD, USA

⁶NASA/Goddard Space Flight Center, Greenbelt, MD 20771, USA

⁷Department of Astronomy and Astrophysics, Pennsylvania State University, University Park, PA 16802, USA

Accepted 2008 October 3. Received 2008 October 3; in original form 2008 July 26

ABSTRACT

IGR J08408–4503 is a supergiant fast X-ray transient discovered in 2006 with a confirmed association with a O8.5Ib(f) supergiant star, HD 74194. We report on the analysis of two outbursts caught by *Swift*/Burst Alert Telescope (BAT) on 2006 October 4 and 2008 July 5, and followed up at softer energies with *Swift*/X-ray Telescope (XRT). The 2008 XRT light curve shows a multiple-peaked structure with an initial bright flare that reached a flux of $\sim 10^{-9}$ erg cm⁻² s⁻¹ (2–10 keV), followed by two equally bright flares within 75 ks. The spectral characteristics of the flares differ dramatically, with most of the difference, as derived via time-resolved spectroscopy, being due to absorbing column variations. We observe a gradual decrease in the N_{H} , derived with a fit using absorbed power-law model, as time passes. We interpret these N_{H} variations as due to an ionization effect produced by the first flare, resulting in a significant decrease in the measured column density towards the source. The durations of the flares as well as the times of the outbursts suggest that the orbital period is ~ 35 d, if the flaring activity is interpreted within the framework of the Sidoli et al. model with the outbursts triggered by the neutron star passage inside an equatorial wind inclined with respect to the orbital plane.

Key words: X-rays: individual: IGR J08408–4503.

1 INTRODUCTION

IGR J08408–4503 belongs to the class of the supergiant fast X-ray transients (SFXTs), which are transient sources in high-mass X-ray binaries (HMXBs) associated with blue supergiant companions (see e.g. Smith et al. 2006). Several members of this class have been discovered since the launch in 2002 of the *INTEGRAL* satellite, thanks to its monitoring of the Galactic plane performed with a large field of view (FOV) and a good sensitivity at hard X-rays. Indeed, several of these transients are highly absorbed in X-rays, and previous missions had failed to detect them (see e.g. Sguera et al. 2005). Two members of this class are X-ray pulsars: IGR J11215–5952 (Swank, Smith & Markwardt 2007) and AX J1841.0–0536/IGR J18410–0535 (Bamba et al. 2001). The X-ray spectra of SFXTs are very similar to those typically displayed by accreting X-ray pulsars, with a flat power-law spectrum below 10 keV and a high-

energy cut-off around 10–30 keV (see Romano et al. 2008, for the first truly simultaneous wide-band X-ray spectrum of a SFXT, from 0.3 to 100 keV). This spectral similarity suggests that the other members of the new class of HMXBs probably host a neutron star as well.

The emerging picture of the SFXTs as a class, especially thanks to more sensitive monitoring performed with *Swift* of four SFXTs (see Sidoli et al. 2008b for the strategy of this ongoing campaign), is that they sporadically undergo bright flares, up to peak luminosities of 10^{36} – 10^{37} erg s⁻¹, with a duration of a few hours for each single flare. This bright flaring activity is actually a part of a much longer duration outburst event, lasting days (see Romano et al. 2007; Sidoli et al. 2008a). Their long-term emission is characterized by a much lower intensity and flaring activity, with an average luminosity of 10^{33} – 10^{34} erg s⁻¹ (Sidoli et al. 2008b). The true quiescence has been rarely observed, and is characterized by a very soft spectrum, with a luminosity as low as 10^{32} erg s⁻¹ (in't Zand 2005; Leyder et al. 2007).

*E-mail: romano@ifc.inaf.it

IGR J08408–4503 was discovered on 2006 May 15, during a short bright flare with a duration of 900 s, reaching a peak flux of 250 mCrab in the 20–40 keV energy band (Götz et al. 2006). Analysis of archival *INTEGRAL* observations of the source field led to the discovery that IGR J08408–4503 is a recurrent transient, being also active on 2003 July 1 (Mereghetti et al. 2006). The refined position with *Swift*/XRT (Kennea & Campana 2006), during a Target of Opportunity observation (ToO) performed about one week after the discovery flare, allowed the confirmation of the association with a O8.5Ib(f) supergiant star, HD 74194, located in the Vela region (Masetti et al. 2006) at a distance of about 3 kpc. Optical spectroscopy of HD 74194 just a few days after the 2006 May 15 flare revealed variability in the H α profile and a radial velocity variation in the He I and He II absorption lines with an amplitude of about 35 km s⁻¹. The study of three additional flares observed with *INTEGRAL* and *Swift* by Götz et al. (2007) led these authors to suggest that the orbital period of IGR J08408–4503 is probably of the order of 1 yr, the spin period of the putative neutron star could be of order of hours and the surface magnetic field is probably around 10¹³ G.

In this paper, we report on the detailed data analysis of both the 2006 October 4 and the 2008 July 5 outbursts caught by *Swift*/BAT and followed up at softer energies with *Swift*/XRT.

2 OBSERVATIONS AND DATA REDUCTION

IGR J08408–4503 triggered the *Swift*/BAT on 2006 October 10 14:45:43 UT (image trigger = 232309) and 2008 July 5 21:14:15 UT (image trigger = 316063; Ward et al. 2008), respectively. On both occasions, *Swift* slewed to the target, allowing the narrow field instruments (NFIs) to be pointing at the target \sim 1885 and \sim 130 s after the trigger, respectively. We note that this source is normally not detectable in the BAT Transient Monitor, but has shown a few untriggered outbursts over the past three years. Table 1 reports the log of the *Swift*/XRT observations used for this work.

The XRT data were processed with standard procedures (XRT-PIPELINE v0.11.6), filtering and screening criteria by using FTOOLS in the HEASOFT package (v.6.4). We considered both Windowed Timing (WT) and Photon Counting (PC) data, and selected event grades 0–2 and 0–12, respectively (Burrows et al. 2005). When appropriate (observations 00232309000 and 00316063000), we corrected for pileup by determining the size of the point spread function

(PSF) core affected by comparing the observed and nominal PSF (Vaughan et al. 2006), and excluding from the analysis all the events that fell within that region. Ancillary response files were generated with XRTMKARF, and they account for different extraction regions, vignetting and PSF corrections. We used the spectral redistribution matrices v010 in HEASARC Calibration Database (CALDB).

The BAT always observed IGR J08408–4503 simultaneously with XRT, so survey data products, in the form of Detector Plane Histograms (DPH) with typical integration time of \sim 300 s, are available. Furthermore, event data were collected during observation 00316063000. The BAT data were analysed using the standard BAT analysis software distributed within FTOOLS. BAT mask-weighted spectra were extracted over the time intervals simultaneous with XRT data (see Section 3.2). Response matrices were generated with BATDRMGEN using the latest spectral redistribution matrices and the default computation method (METHOD = MEAN) accessing calibration parameters (Markwardt et al. 2007) that are averaged over the entire BAT FOV. For our spectral fitting (XSPEC v11.3.2), we applied an energy-dependent systematic error, amounting to 4–5 per cent through all the 15–90 keV energy band (Markwardt et al. 2007). Inspection of the BAT FOV shows that no source substantially brighter than IGR J08408–4503 was visible during both the 2006 and 2008 observations, and we can estimate that possible contamination from other sources in the FOV cannot exceed 5 per cent.

Ultraviolet/Optical Telescope (UVOT) data were also collected simultaneously with the other instruments; however, due to the brightness of HD 74194 (LM Vel), the data were not usable in order to study the variability of the optical counterpart.

All quoted uncertainties are given at 90 per cent confidence level for one interesting parameter unless otherwise stated. The spectral indices are parametrized as $F_\nu \propto \nu^{-\alpha}$, where F_ν (erg cm⁻² s⁻¹ Hz⁻¹) is the flux density as a function of frequency ν ; we adopt $\Gamma = \alpha + 1$ as the photon index, $N(E) \propto E^{-\Gamma}$ (ph cm⁻² s⁻¹ keV⁻¹). Times in the light curves and the text are referred to their respective triggers.

3 ANALYSIS AND RESULTS

3.1 Light curves

For both observations 00232309000 (2006 outburst) and 00316063000 (2008), XRT light curves were extracted in several

Table 1. Observation log.

Sequence	Instrument /mode	Start time (UT) (yyyy-mm-dd h:m:s)	End time (UT) (yyyy-mm-dd h:m:s)	Exposure ^a (s)
00232309000	XRT/WT	2006-10-04 15:17:16	2006-10-04 16:51:12	180
00232309000	XRT/PC	2006-10-04 15:20:08	2006-10-04 17:05:56	1472
00232309001	XRT/PC	2006-10-04 18:27:05	2006-10-04 18:42:58	951
00316063000	XRT/PC	2008-07-05 21:18:23	2008-07-06 18:29:51	29956
00316063000	XRT/WT	2008-07-05 21:16:31	2008-07-06 17:55:16	447
00030707003	XRT/PC	2008-07-08 13:26:02	2008-07-08 18:23:18	1978
00030707004	XRT/PC	2008-07-09 18:26:26	2008-07-09 18:43:04	998
00030707005	XRT/PC	2008-07-10 23:12:51	2008-07-10 23:28:56	965
00030707006	XRT/PC	2008-07-11 00:55:02	2008-07-11 02:41:57	1308
00030707007	XRT/PC	2008-07-12 20:25:43	2008-07-12 22:14:56	1319
00030707008	XRT/PC	2008-07-14 20:28:10	2008-07-14 23:47:51	1203
00030707009	XRT/PC	2008-07-15 04:30:10	2008-07-15 23:51:55	2384
00030707010	XRT/PC	2008-07-16 19:03:10	2008-07-16 23:59:57	1474
00030707011	XRT/PC	2008-07-17 22:27:20	2008-07-17 22:38:25	664
00030707012	XRT/PC	2008-07-20 11:37:03	2008-07-20 11:56:56	1193

^aThe exposure time is spread over several snapshots (single continuous pointings at the target) during each observation.

energy bands using the procedures described in Evans et al. (2007). Mask-tagged BAT light curves were created in the standard four energy bands, 15–25, 25–50, 50–100 and 100–150 keV, for observation 00316063000, and rebinned to achieve a signal-to-noise ratio (S/N) of 10. Fig. 1 shows the XRT light curves for the 2006 outburst, while Figs 2 and 3 show the BAT and XRT light curves for the 2008 outburst, respectively. As shown in Fig. 1, the late start of the 2006 XRT observation (T+1885 s) only allowed us to follow the descent of the outburst. In contrast, the XRT 2008 data offer a much better coverage and show a remarkable second and third flares, which reached the same intensity as the first one.

Figs 1c and 3d show the 4–10/1–4 hardness ratios. Fitting the 2006 XRT hardness ratio against a constant yields a value of 0.60 ± 0.02 [$\chi^2_\nu = 1.64$ for 33 degrees of freedom (d.o.f.)], which corresponds a $\sim 2.5\sigma$ variation. In the case of the 2008 XRT data, we see a definite trend for a softening of the spectrum as the source

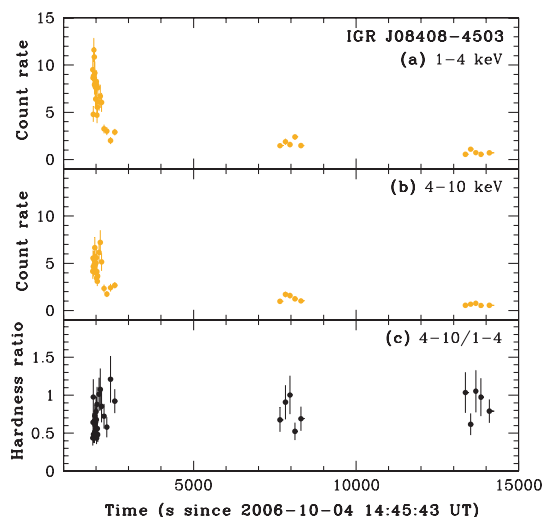


Figure 1. XRT light curves of the 2006 October 4 outburst background subtracted and corrected for pile up, PSF losses and vignetting, rebinned with a minimum of 30 counts per bin: (a) 1–4 keV band; (b) 4–10 keV energy band and (c) 4–10/1–4 hardness ratio.

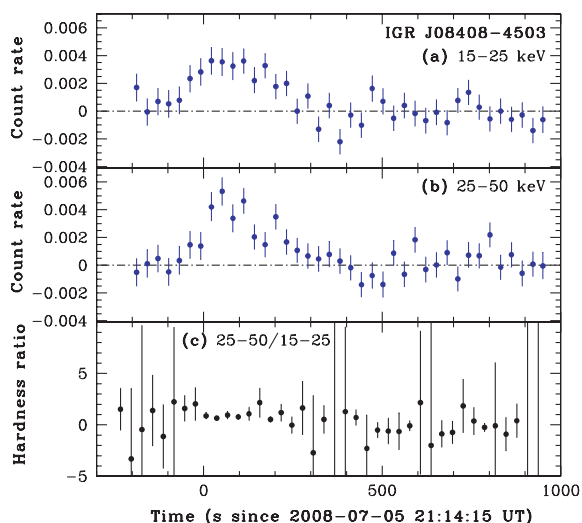


Figure 2. BAT light curves of the 2008 July 5 outburst, rebinned at a S/N = 10. (a) 15–25 keV band (units of counts $s^{-1} \text{det}^{-1}$); (b) 25–50 keV band (counts $s^{-1} \text{det}^{-1}$) and (c) 25–50/15–25 hardness ratio.

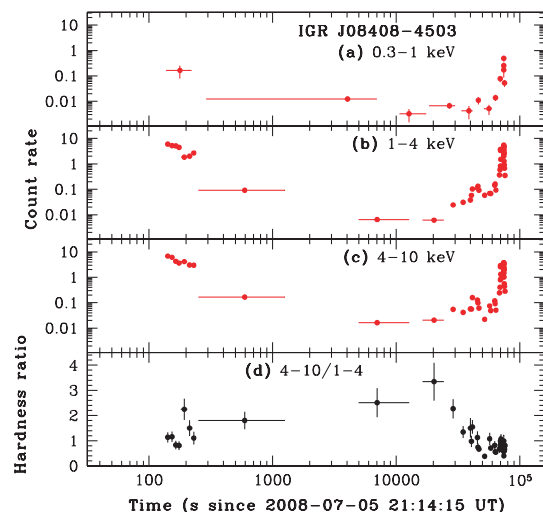


Figure 3. XRT light curves of the 2008 July 5 outburst rebinned with a minimum of 30 counts per bin: (a) 0.3–1 keV band; (b) 1–4 keV band; (c) 4–10 keV energy band and (d) 4–10/1–4 hardness ratio.

becomes brighter, which is reminiscent of what was observed, albeit with lower statistics, during the 2008 March 19 outburst of IGR J16479–4514 (Romano et al. 2008). No significant variation in the 2008 BAT hardness ratio is evident (Fig. 2c). Fitting the hardness ratio as a function of time to a constant model we obtain a value of 0.58 ± 0.11 ($\chi^2_\nu = 0.56$ for 39 d.o.f.).

A timing analysis was performed on WT data, after having converted the event arrival times to the Solar system barycentric frame. We searched for coherent periodicity, but found no evidence for pulsations in the range 10–100 s.

3.2 Broad-band spectra

For the 2006 October 4 outburst, we extracted one BAT spectrum nearly simultaneous with the XRT/WT data set and performed a broad-band fit to an absorbed power law with an exponential cut-off. The XRT data were rebinned with a minimum of 20 counts per energy bin to allow χ^2 fitting, while the BAT data were rebinned to a S/N > 5. We fit in the 0.3–10 and 15–80 keV energy ranges for the XRT and BAT data, respectively, with XSPEC (v11.3.2). Similarly, we extracted a BAT spectrum simultaneous with the XRT/WT data (137–246 s) for the 2008 July 5 outburst. The best-fitting parameters are reported in Table 2, while the spectra are shown in Figs 4 and 5, respectively. We note that there are no BAT event data during the second and third flares of the 2008 light curve, since the source was already identified on board as the current automated target and it did not reach the required count rate (twice the previous triggering rate plus 7σ) to trigger the BAT again. We also note that the presence of a cut-off is required by the data, since the trend in the residuals of a simple power-law model clearly indicates the presence of curvature in the spectrum.

Table 2. Broad-band spectral fits of the BAT+XRT data.

Year	N_H (10^{22}cm^{-2})	Γ	E_c (keV)	$\chi^2_\nu/\text{d.o.f.}$
2006	$0.29^{+0.17}_{-0.14}$	$0.31^{+0.23}_{-0.23}$	11^{+4}_{-3}	0.903/69
2008	$6.7^{+2.0}_{-1.8}$	$1.36^{+0.49}_{-0.56}$	> 14	1.191/45

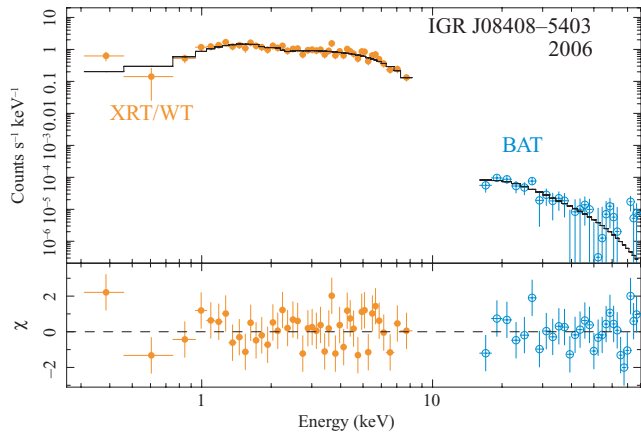


Figure 4. Spectroscopy of the 2006 October 4 outburst. Top panel: simultaneous fit of BAT and XRT/WT data with an absorbed power law with a high-energy cut-off. Bottom panel: the residuals of the fit (in units of standard deviations).

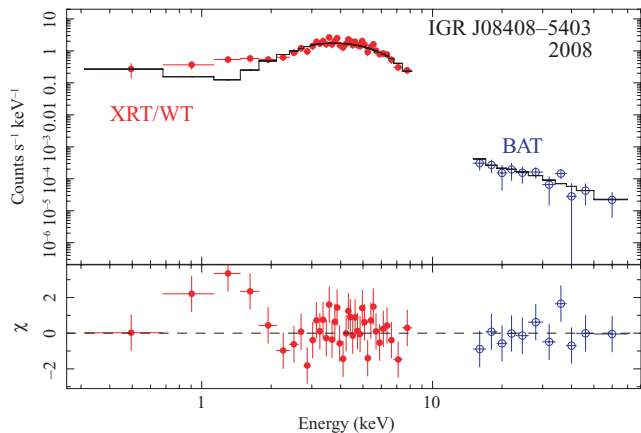


Figure 5. Spectroscopy of the 2008 July 5 outburst. Top panel: simultaneous fit of BAT and XRT/WT data with an absorbed power law with a high-energy cut-off. Bottom panel: the residuals of the fit (in units of standard deviations).

3.3 Time-resolved spectra

Upon examination of the light curve and the available counting statistics, we selected different time bins over which we accumulated spectra. For the 2006 data, we extracted one spectrum in WT mode and two in PC mode (observations 00232309000 and 00232309001 in Table 1). For the 2008 data, our time selections include (see Fig. 6a, c and Table 3): (i) the initial WT data (137–246 s, hereafter WT1); (ii) a low phase, with a mean CR $\sim 3.5 \times 10^{-2}$ counts s⁻¹ (4762–30180 s, orbits 2–6 of observation 00316063000, PC1); (iii) an intermediate phase, with a mean CR ~ 0.1 counts s⁻¹ (33697–64903 s, orbits 7–12, PC2); (iv) the second flare (68 429–70 690 s, orbit 13, PC3); (v) the rise of the third flare (74208–74462 s, orbit 14, WT4) and (vi) the decay of the third flare (74 463–76 477 s, orbit 14, PC5). The spectra were rebinned with a minimum of 20 counts per energy bin to allow χ^2 fitting (see Fig. 6c). However, the Cash statistic (Cash 1979) and spectrally unbinned data were used, due to the low counting statistics, to fit the PC1 spectrum (the unbinned spectrum is not shown Fig. 7). Each spectrum was fit in the 0.3–10 keV energy range, adopting an absorbed power-law model. The best-fitting param-

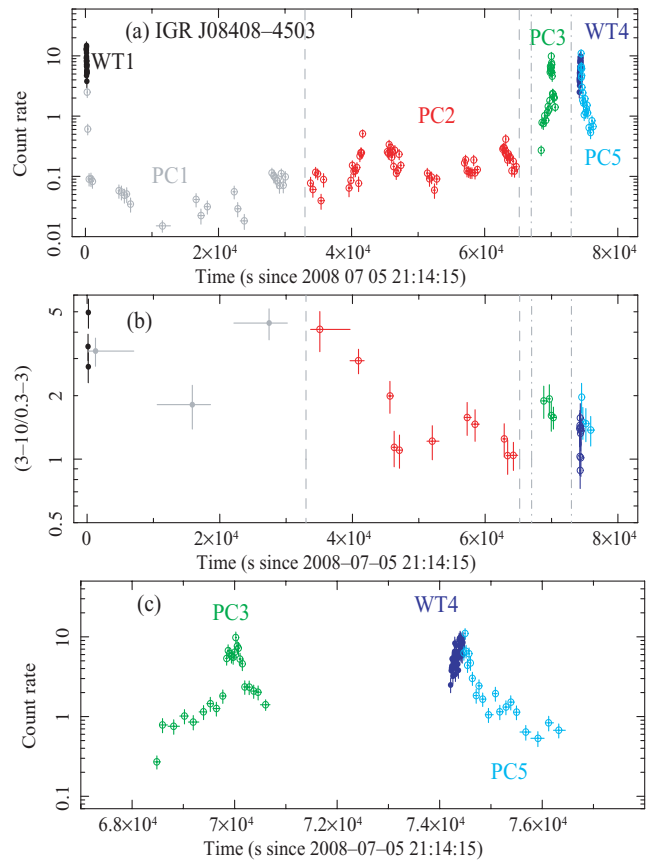


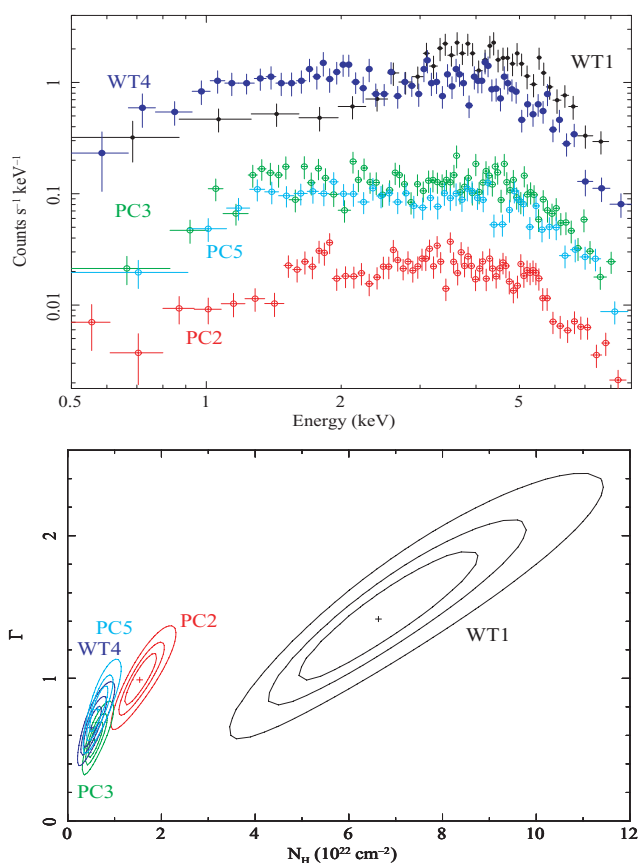
Figure 6. Time selections for XRT spectroscopy of the 2008 July 5 outburst. (a) XRT 0.3–10 keV light curve; the intervals over which we performed spectroscopy are marked with vertical lines and labels. (b) 3–10/0.3–3 keV hardness ratio. (c) Detail of (a) to show the second and third flare.

eters are reported in Table 3. Remarkably, we obtain significantly different fitting parameters for the data of the three flares, despite quite similar flux levels. Indeed, for the first one (WT1) we obtain a photon index $\Gamma_{\text{WT1}} = 1.42^{+0.52}_{-0.47}$ and an absorbing column density of $N_{\text{HWT1}} = (6.63^{+2.34}_{-1.88}) \times 10^{22}$ cm⁻², while the second and third ones (PC3, WT4/PC5) yielded $\Gamma_{\text{WT4}} = 0.65^{+0.17}_{-0.15}$ and $\Gamma_{\text{PC5}} = 0.78^{+0.18}_{-0.17}$, and an absorbing column density of $N_{\text{HWT4}} = (0.50^{+0.24}_{-0.18}) \times 10^{22}$ cm⁻² $N_{\text{HPC5}} = (0.64^{+0.24}_{-0.19}) \times 10^{22}$ cm⁻². Fig. 7 (bottom panel) shows the contour levels for the column density versus the photon index, which we created to investigate these spectral variations. As can be seen, the photon index range is restricted to $\Gamma \approx 1 \pm 0.5$, while the measured absorbing column varies by an order of magnitude with a definite trend for a decreasing N_{H} as time goes by. It must also be noted that the 2006 spectra, taken about 2000 s from the trigger, are quite similar to these ‘late’ (PC3 onwards) spectra. We note the presence of a bump in the residuals at soft energies around 1 keV (see Fig. 5). This feature, which has a variable contribution to the spectra and is stronger in WT1, is probably due to a combination of a slight spectral variability throughout the time interval during which the spectrum was accumulated (see Figs 3d and 6b) and some residual calibration uncertainties below 2 keV in WT data (Godet et al. 2008). We are, however, confident that the latter do not weaken our findings of a decreasing N_{H} , since their effect is in the opposite direction and we will not discuss this feature any further.

Table 3. Spectral fits of the XRT data.

Year	Spectrum	Times (s)	N_{H} (10^{22} cm^{-2})	Γ	Flux ^a	$\chi^2_{\nu}/\text{d.o.f.}$
2006	WT	1893–2064	$0.37^{+0.17}_{-0.14}$	$0.67^{+0.17}_{-0.17}$	5.7	0.902/42
	PC000	2064–8413	$0.90^{+0.35}_{-0.28}$	$0.88^{+0.24}_{-0.22}$	1.4	1.477/31
	PC001	13283–14234	$0.47^{+0.41}_{-0.27}$	$0.49^{+0.30}_{-0.26}$	1.5	0.554/19
	all	1893–14234	$0.57^{+0.15}_{-0.13}$	$0.69^{+0.13}_{-0.12}$		1.118/96
2008	WT1	137–246	$6.63^{+2.34}_{-1.88}$	$1.42^{+0.52}_{-0.47}$	13.4	1.255/35
	PC1	4762–30180	$11.08^{+5.12}_{-4.20}$	$0.65^{+0.75}_{-0.69}$	0.086	578.4 (55.78 per cent) ^b
	PC2	33697–64903	$1.54^{+0.40}_{-0.33}$	$0.99^{+0.20}_{-0.19}$	0.14	1.423/70
	PC3	68429–70690	$0.57^{+0.20}_{-0.16}$	$0.57^{+0.14}_{-0.14}$	1.8	1.368/70
	WT4	74208–74462	$0.50^{+0.24}_{-0.18}$	$0.65^{+0.17}_{-0.15}$	5.3	1.371/62
	PC5	74463–76477	$0.64^{+0.24}_{-0.19}$	$0.78^{+0.18}_{-0.17}$	1.3	0.829/44

^aUnabsorbed 2–10 keV flux in units of $10^{-10} \text{ erg cm}^{-2} \text{ s}^{-1}$.

^bCash statistics Cstat and percentage of realizations (10^4 trials) with statistic > Cstat.

Figure 7. XRT time-selected spectroscopy of the 2008 July 5 outburst. Top panel: spectra extracted in the different intervals. Bottom panel: 68, 90 and 99 per cent confidence level contours adopting an absorbed power-law model. The labels refer to the time intervals shown in Fig. 6 and Table 3.

4 DISCUSSION AND CONCLUSIONS

4.1 Multiple flaring behaviour

In this paper, we report on two outbursts of the SFXT IGR J08408–4503 observed by *Swift* on 2006 October 4 and 2008

July 5. During the 2008 outburst, a multiple-flare behaviour is observed so clearly in a SFXT, and for the first time with a large dynamic range, thanks to the good sampling of the source light curve. The 2008 outburst emission is composed of three main bright flares, each exceeding $10^{36} \text{ erg s}^{-1}$, with a duration of a few hundred seconds. The flares are separated by ~ 70 ks (between the first and second flare) and ~ 4 ks (second to third flare).

Structured and complex peaks during outburst flares have already been observed in other SFXTs [see e.g. the flaring activity observed during the brightest phase of the outburst in IGR J11215–5952 (Romano et al. 2007), or the several flares caught in XTE J1739–302 with *Swift* (Sidoli et al. 2008a) and *INTEGRAL* at different epochs (Blay et al. 2008)]. However, it has never been observed spanning almost three orders of magnitude in flux, as found between the first two flare peaks in 2008 (WT1 and PC3 data set in Fig. 6, exceeding 10 counts s^{-1}) and their interflare emission (PC1, which goes down to ~ 0.01 counts s^{-1}). The hardness ratios (Fig. 3d and 6b) show an anticorrelation with the source intensity, and our time-selected spectroscopy demonstrates that this evolution is produced by a change in the absorbing column density, instead of a change in the source spectrum (Fig. 7). In particular, there is evidence for a progressively decreasing column density with time (also during the low intensity emission of the part PC2 of the light curve). This is strongly suggestive of an ionization effect produced by the first flare, resulting in a significant decrease in the measured column density towards the source.

During the first flare in 2008, BAT events were also available and a broad-band spectrum could be extracted (see Table 3); however during the second and third flares, BAT did not trigger (see Section 3.2) and the source was only detected at the $\sim 6\sigma$ level in survey data, so no broad-band coverage is available. The broad-band spectra during the two flares in 2006 and 2008 are significantly different, especially as far as the absorbing column density is concerned, which was about 20 times higher in the first flare in 2008 than during the 2006 flare [where the absorption is consistent with the interstellar value of $3 \times 10^{21} \text{ cm}^{-2}$ derived from the optical extinction to the optical counterpart HD 74194 (Leyder et al. 2007)]. We note that the 2006 flare spectrum was extracted about 2000 s after the BAT trigger; *Swift* made a delayed slew to the source, too late to catch the peak of the first flare which triggered the BAT. This implies that the low column density observed during the 2006

flare is probably so low when compared with the first 2008 flare (WT1, taken only 137 s after the BAT trigger), only because of the ionization effect caused by the flare that triggered the BAT (and not observed by XRT).

This suggests that, during extended bright flaring activity, it is not possible to directly derive the mass of the clump which is supposed to produce the enhanced accretion luminosity, in the framework of the clumpy stellar wind model (Walter & Zurita Heras 2007), because part or all of the accreting material could have been ionized by a previous bright flare (as in 2006, where the presence of a precursor flare is deduced from the fact it triggered the BAT).

The broad-band spectrum during the 2006 flare is well fitted with a power law with a high-energy cut-off at ~ 11 keV. This is compatible with a surface magnetic field of a typical X-ray pulsar (Coburn et al. 2002), around 10^{12} G, much lower than that suggested by Bozzo, Falanga & Stella (2008) or by Götz et al. (2007).

The interflare emission is highly variable, showing a trend with an average decreasing flux after the first flare (for about 10 ks), then continuously increasing by an order of magnitude (with a low intensity flaring activity, see PC2 part) up to the second flare. The spectrum in this lower intensity interflare emission is well fitted with a hard power law with a photon index of ~ 1 , which implies that accretion is still present. The true quiescence has been observed by Leyder et al. (2007), and displays a much softer spectrum and a lower luminosity around $\sim 10^{32}$ erg s $^{-1}$. This interflare emission is probably due to the accretion of interclump medium, implying a density (and/or a velocity) contrast in the supergiant wind of at least 10^3 , which is not unusual in line-driven winds. Indeed, in recent years, evidence has been accumulated that hot stellar winds are not smooth, as previously thought, but highly inhomogeneous (see e.g. Oskinova, Hamann & Feldmeier 2007 and references therein), thus implying important consequences, for example, in the mass-loss rate determination, and also in the stellar evolution.

4.2 Clumpy winds model: an estimate of the neutron star distance from the supergiant companion

This new *Swift* data set interestingly allows us to accurately determine the flare duration, particularly of the second (PC3 data) and third flares (WT4/PC5). Fitting their light curves with Gaussian profiles, we derive a full width at half-maximum of 370 ± 20 and 500 ± 30 s, respectively. These durations can be used to derive information about the distance of the neutron star from the supergiant companion during the outburst, since the clump sizes increase with the distance from the supergiant star, as follows. The size of a clump is determined by the balance pressure equation. Following Lucy & White (1980) and Howk et al. (2000), the average density of a clump is

$$\bar{\rho}_c = \rho_w(r) \left(\frac{a_w^2 + C_\rho \omega^2}{a_c^2} \right), \quad (1)$$

where $\rho_w(r)$ is the density profile of the homogeneous (interclump) wind, a_w and a_c are the interclump wind and the clump thermal velocity, respectively: $a_w^2 = \frac{kT_w}{\mu m_H}$ and $a_c^2 = \frac{kT_c}{\mu m_H}$, where k is the Boltzmann constant, T_w and T_c are the temperatures of the interclump wind and the clump, respectively. The constant $C_\rho = 0.29$ accounts for the confining effect of the bow shock produced by the ram pressure around the clump (Lucy & White 1980), while ω is the relative velocity between the wind and the clump ($\omega = v_w - v_c$).

Wind structure simulations show that the average relative velocity $\bar{\omega}$ is $\sim 5 \times 10^7$ cm s $^{-1}$, the average clump temperature is $\bar{T}_c \sim 10^5$ K and the average temperature of the homogeneous interclump wind is $\bar{T}_w \sim 10^7$ K (Runacres & Owocki 2005). Adopting these values for T_c , T_w , ω and $\mu = 1.3$ (for solar abundances), we obtain

$$\left(\frac{a_w^2 + C_\rho \omega^2}{a_c^2} \right) \approx 200. \quad (2)$$

Since the density radial profile $\rho_w(r)$ of the homogeneous interclump wind is

$$\rho_w(r) = \rho_w(R_{OB}) \frac{R_{OB}^2 v(R_{OB})}{r^2 v(r)}, \quad (3)$$

where R_{OB} is the radius of the supergiant ($R_{OB} = 23.8 R_\odot$, Vacca, Garmany & Shull 1996), then from equations (1–3), we obtain

$$\bar{\rho}_c(r) = \bar{\rho}_c(R_{OB}) \frac{R_{OB}^2 v(R_{OB})}{r^2 v(r)}, \quad (4)$$

where $\bar{\rho}_c(R_{OB}) = \rho_w(R_{OB}) \times 200$. Assuming a spherical geometry for the clumps, it is possible to obtain the expansion law of the clump from equation (4):

$$R_c(r) = R_c(R_{OB}) \left[\frac{r^2 v(r)}{R_{OB}^2 v_0} \right]^{1/3}, \quad (5)$$

where $v_0 = v(R_{OB})$ is the initial velocity of the clump at the surface of the supergiant, which can be assumed $v_0 = 10$ km s $^{-1}$ (Castor, Abbott & Klein 1975). For $v(r)$, we consider the standard β law for the velocity profile in line-driven winds, with a terminal velocity of 1900 km s $^{-1}$ and an exponent $\beta = 0.8$.

The flare duration t is linked with the thickness of the clump, therefore

$$t \approx \frac{2R_c}{v_c} = \frac{2R_c(R_{OB})}{v_c} \left[\frac{r^2 v(r)^2}{R_{OB}^2 v_0} \right]^{1/3}, \quad (6)$$

where we assumed $R_c(R_{OB}) \approx 2 \times 10^9$ cm; thus, flare durations of the order of ~ 500 s can be produced at a radial distance of $\sim 5R_{OB}$ (or 10^{13} cm), which implies an orbital period of ~ 35 d, assuming a companion mass of $30 M_\odot$. This estimate is in agreement with that obtained by Leyder et al. (2007), but is significantly shorter than what calculated by Götz et al. (2007).

4.3 The orbital period and the outbursts double periodicity

We note that the first three outbursts reported in the literature (on 52821, 53870 and 54012 MJD) are indeed spaced by a multiple of 35 d (30 and 34 cycles, respectively, after the first observed outburst on 52821 MJD). On the other hand, the 2008 outburst (54652 MJD) does not occur strictly after an integer number of cycles with this assumed period. This suggested to try different combinations of two numbers (two subperiods P_1 and P_2 , such that $P = P_1 + P_2 = 35$ d) to test the possibility, suggested in Sidoli et al. (2007), that the SFXTs outbursts occur with a double periodicity, when the neutron star crosses the equatorial wind of the companion twice along the eccentric orbit (see their fig. 9c). In this hypothesis, the times of the n_{th} outburst is given by $t_n = t_0 + (n_1 P_1) + (n_2 P_2)$. Among the several couples of numbers we tried (with sum equal to 35 d), we find that $P_1 = 11$ and $P_2 = 24$ d well account for all the four reported outburst times (calculated with $n_1 = n_2 = 30$, $n_1 = n_2 = 34$ and with $n_1 = 53$ and $n_2 = 52$, respectively for the three outbursts, assuming $t_0 = 52821$ MJD), within an uncertainty of 1 d.

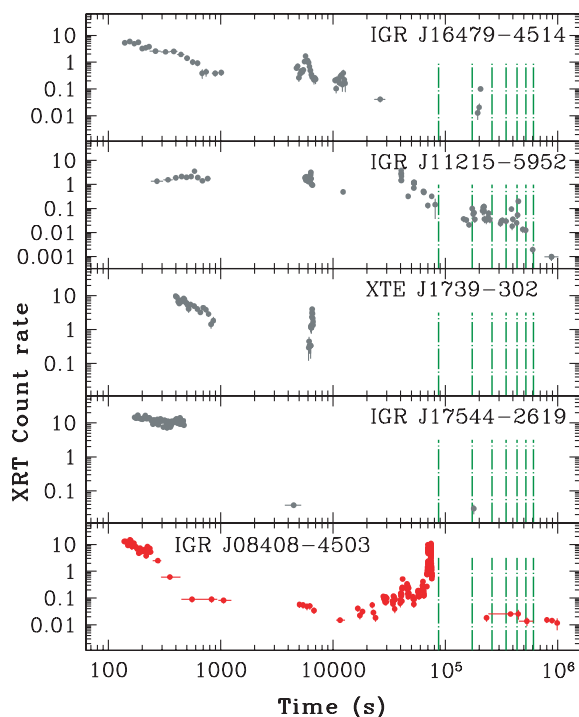


Figure 8. Light curves of the outbursts of SFXTs followed by *Swift*/XRT referred to their respective triggers. We show the 2005 outburst of IGR J16479–4514 (Sidoli et al. 2008b), which is more complete than the one observed in 2008 (Romano et al. 2008). The IGR J11215–5952 light curve has an arbitrary start time, since the source did not trigger the BAT (the observations were obtained as a ToO; Romano et al. 2007). The data on XTE J1739–302 and IGR J17544–2619 are presented in Sidoli et al. (2008a). Note that where no data are plotted, no data were collected. For clarity, we drew dashed vertical lines to mark each day (up to one week) since the trigger.

4.4 IGR J08408–4503 in the SFXT context

The multiple flares we observe here, reaching similar peak luminosities, cover about one day of bright outburst emission and are then followed by lower X-ray emission in the subsequent days, similar to what we already observed in four other SFXTs with *Swift* (see Fig. 8). The three flares observed here so close in time, after a long period during which no bright flares have been observed, are suggestive of the fact that the neutron star is probably crossing a region of higher average density of the wind, compatible with the model we proposed for IGR J11215–5952 (Sidoli et al. 2007). In this hypothesis, the outbursts in SFXTs are produced when the neutron star crosses an equatorially enhanced region of the supergiant companion, which is inclined with respect to the orbital plane. The different flares then are probably produced by inhomogeneities in the structure of the wind, which, in our proposed model, is anisotropic, showing a preferential plane along the equator of the supergiant companion. This could explain why the flares happen in a preferential region of the neutron star orbit, displaying a particularly high X-ray flare rate. New observations during the next outbursts are crucial in order to test this hypothesis and to confirm whether multiple outbursts are indeed a usual property of this (and other) SFXTs, and if there is indeed an orbital phase dependence of the X-ray flare rate.

ACKNOWLEDGMENTS

We thank the *Swift* team for making these observations possible, the duty scientists and science planners. We also thank the anonymous referee for comments that helped improve the paper. This work was supported in Italy by contracts ASI/INAF I/088/06/0 and I/023/05/0. APB, PAE and KLP acknowledge STFC support. HAK was supported by the *Swift* project. DNB and JAK acknowledge support from NASA contract NAS5-00136.

REFERENCES

- Bamba A., Yokogawa J., Ueno M., Koyama K., Yamauchi S., 2001, *PASJ*, 53, 1179
 Blay P. et al., 2008, *A&A*, 489, 699
 Bozzo E., Falanga M., Stella L., 2008, *ApJ*, 683, 1031
 Burrows D. N. et al., 2005, *Space Sci. Rev.*, 120, 165
 Cash W., 1979, *ApJ*, 228, 939
 Castor J. I., Abbott D. C., Klein R. I., 1975, *ApJ*, 195, 157
 Coburn W., Heindl W. A., Rothschild R. E., Gruber D. E., Kreykenbohm I., Wilms J., Kretschmar P., Staubert R., 2002, *ApJ*, 580, 394
 Evans P. A. et al., 2007, *A&A*, 469, 379
 Godet O. et al., 2008, *A&A*, submitted
 Götz D., Schanne S., Rodriguez J., Leyder J.-C., von Kienlin A., Mowlavi N., Mereghetti S., 2006, *Astron. Tel.*, 813
 Götz D., Falanga M., Senziani F., De Luca A., Schanne S., von Kienlin A., 2007, *ApJ*, 655, L101
 Howk J. C., Cassinelli J. P., Bjorkman J. E., Lamers H. J. G. L. M., 2000, *ApJ*, 534, 348
 in't Zand J. J. M., 2005, *A&A*, 441, L1
 Kennea J. A., Campana S., 2006, *Astron. Tel.*, 818
 Leyder J.-C., Walter R., Lazos M., Masetti N., Produit N., 2007, *A&A*, 465, L35
 Lucy L. B., White R. L., 1980, *ApJ*, 241, 300
 Markwardt C. B., Barthelmy S., Cummings J. R., Hullinger D., Krimm H. A., Parsons A., 2007, in 'The SWIFT BAT Software Guide (Version 6.3)' (http://swift.gsfc.nasa.gov/docs/swift/analysis/bat_swguide_v6_3.pdf)
 Masetti N., Bassani L., Bazzano A., Dean A. J., Stephen J. B., Walter R., 2006, *Astron. Tel.*, 815
 Mereghetti S., Sidoli L., Paizis A., Gotz D., 2006, *Astron. Tel.*, 814
 Oskinova L. M., Hamann W.-R., Feldmeier A., 2007, *A&A*, 476, 1331
 Romano P., Sidoli L., Mangano V., Mereghetti S., Cusumano G., 2007, *A&A*, 469, L5
 Romano P. et al., 2008, *ApJ*, 680, L137
 Runacres M. C., Owocki S. P., 2005, *A&A*, 429, 323
 Sguera V. et al., 2005, *A&A*, 444, 221
 Sidoli L., Romano P., Mereghetti S., Paizis A., Vercellone S., Mangano V., Götz D., 2007, *A&A*, 476, 1307
 Sidoli L. et al., 2008a, *ApJ*, 687, 1230
 Sidoli L. et al., 2008b, *ApJ*, in press (arxiv:0805.1808)
 Smith D. M., Heindl W. A., Markwardt C. B., Swank J. H., Negueruela I., Harrison T. E., Huss L., 2006, *ApJ*, 638, 974
 Swank J. H., Smith D. M., Markwardt C. B., 2007, *Astron. Tel.*, 999
 Vacca W. D., Garmany C. D., Shull J. M., 1996, *ApJ*, 460, 914
 Vaughan S. et al., 2006, *ApJ*, 638, 920
 Walter R., Zurita Heras J., 2007, *A&A*, 476, 335
 Ward P. A. et al., 2008, *GCN Circ.*, 7945

This paper has been typeset from a $\text{\TeX}/\text{\LaTeX}$ file prepared by the author.